HEALED OR NON-HEALED? COMPUTED TOMOGRAPHY (CT) VISUALISATION OF MORPHOLOGY OF BITE TRACE ICHNOTAXA ON A DINOSAUR BONE

Aase Roland JACOBSEN[1], Henrik LAURIDSEN[2], Bente FIIRGAARD[3], Lene Warner Thorup BOEL[4] & Kasper HANSEN[2]

[1] *The Steno Museum, Aarhus University, C.F. Moellers Alle 2, DK-8000 Aarhus C, Denmark; e-mail: aase.jacobsen@si.au.dk*
[2] *Comparative Medicine Lab, Aarhus University, Palle Juul-Jensens Boulevard 99, DK-8200, Aarhus N, Denmark;*
e-mails: K. Hansen: kasperhansen@clin.au.dk and H. Lauridsen: henrik@clin.au.dk
[3] *Department of Radiology, Aarhus University Hospital, Palle Juul-Jensens Boulevard 99, DK-8200, Aarhus N, Denmark;*
e-mail: bentfiir@rm.dk
[4] *Department of Forensic Medicine, Aarhus University, Palle Juul-Jensens Boulevard 99, DK-8200, Aarhus N, Denmark;*
e-mail: lwb@forens.au.dk

Abstract: Bite traces on fossilised bones can provide important information on predator-prey relations and interactions in ancient environments. In 2009, two new ichnotaxa, *Linichnus serratus* and *Knethichnus parallelum*, were introduced to develop the application of bite traces as an ichnological tool. Ichnotaxa defined by theropod bite traces can provide useful information for understanding feeding behaviour. However, objective interpretation of possible bite traces can be difficult using traditional visual inspection. In this study, the bite traces on a fossilised dinosaur bone were comprehensively examined by correlating traditional naked-eye inspection with computed tomography (CT) imaging, used to visualise the internal morphology of the bite traces and in particular, to clarify the appearance of one possibly healed bite trace. A forensic pathologist visually examined the bone with the aid of stereomicroscopy and a radiologist analysed the CT scans. Sixteen different scanner settings were used to optimise the CT parameters and avoid signal attenuation, in the form of hypointense artefacts in the central trabeculated part of the bone fragment. The use of CT scanning provided information on internal morphology from the vicinity of the bite trace, including hyperdense zones, not identified using visual inspection alone. By applying the extended CT scale, the dense and radiopaque cortical bone layer could be clearly identified and applied as a pathomorphological marker to correctly distinguish non-healed from healed wounds. In conclusion, the authors demonstrate that external visual examination of trace fossils by ichnologists in combination with interior examination using CT imaging can be applied to characterise ichnotaxa defined by bite traces and potentially provide clues on ancient feeding behaviour.

Key words: Bite traces, dinosaur bone, theropod, CT, stereomicroscopy.

INTRODUCTION

Traces on dinosaur bones include muscle impressions, trample marks, signs of diseases, injuries, and bite traces. Several studies of bite traces on dinosaur bones, using traditional visual inspection and microscopy, have provided insight into feeding behaviour. For example, the bite force of a Tyrannosaurus has been estimated from bite traces (Erickson and Olson, 1996; Erickson *et al.*, 1996). In addition, bone consumption patterns have provided information on feeding strategy and prey preferences for theropods (Fiorillo, 1991; Jacobsen, 1998; Rogers *et al.*, 2003; D'Amore and Blumenschine, 2012; Boyd *et al.*, 2013). Studies of

feeding behaviour in present-day predators, such as crocodiles (Erickson and Olson, 1996; Erickson *et al.*, 1996; Njau and Blumenschine, 2012) and Komodo dragons (D'Amore and Blumenschine, 2012), have revealed, that modern bite traces may be correlated with the bite traces found on dinosaur bones, especially in the case of the ichnotaxon *Knethichnus parallelum* (Jacobsen and Bromley, 2009; D'Amore and Blumenschine, 2012).

Ichnotaxa for bioerosion trace fossils have recently been summarised by Pirrone and colleagues (Pirrone *et al.*, 2014), who concluded that a few specific bioerosion trace
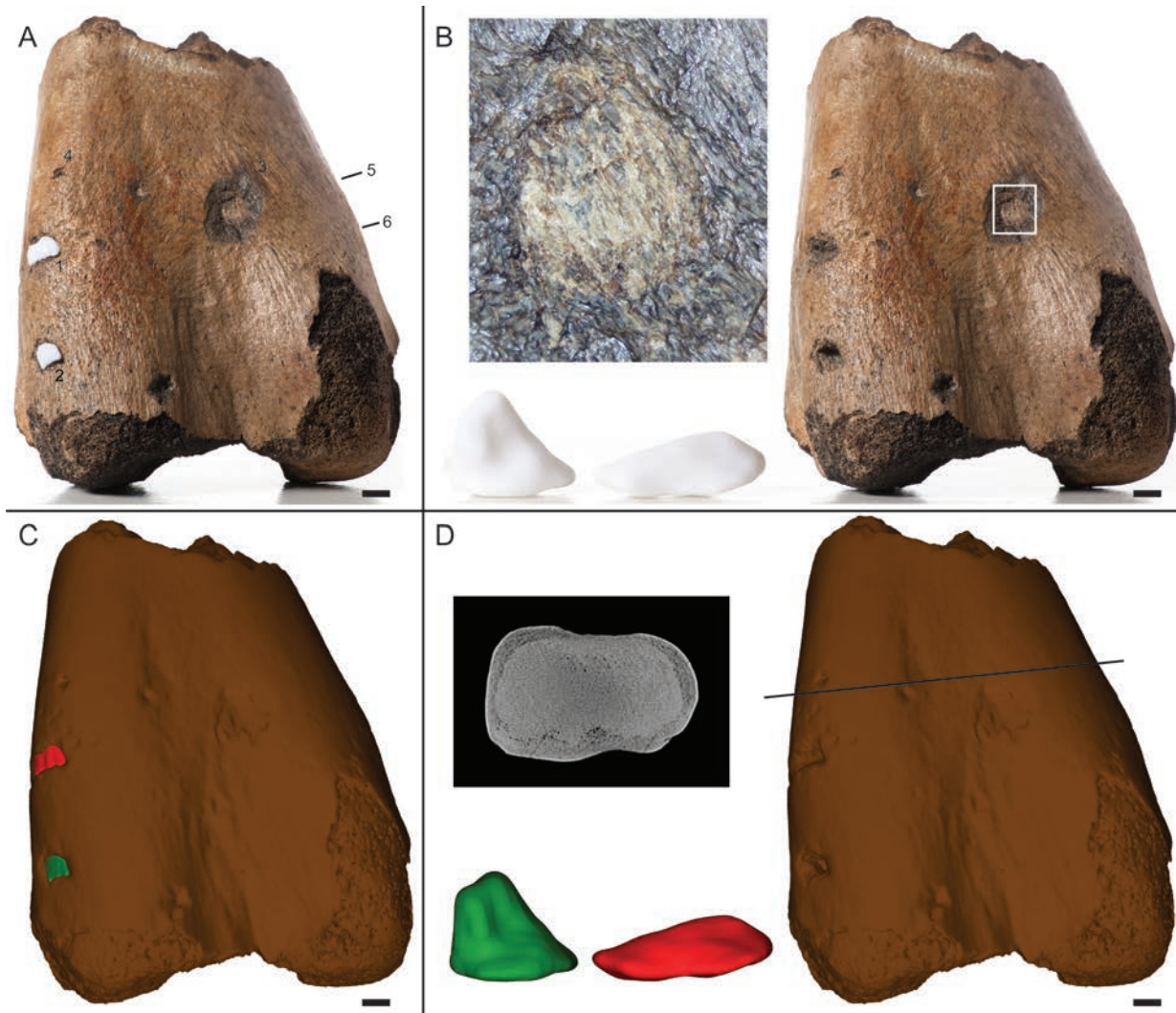
Fig. 1.   Visual inspection, stereomicroscopy and x-ray computed tomography of a hadrosaur (Hadrosauridae sp.) distal femur fragment. Visual inspection (**A, B**) of a fossil specimen can be accompanied by stereomicroscopic examination (B) and x-ray computed tomography (CT) investigation (**C, D**) of reconstructed 3-D models (C) and sections (D). Structures of interest, such as bite traces, can be segmented from CT data and used to generate virtual 3-D models (C, D) and 3-D prints of scale models (A, B). Scale bar is 1 cm. 3-D-printed models in A are not scaled and naturally fit inside the fossil, whereas prints in B are scaled to 400% to enhance morphological interpretation.

fossils in bones even present the potential for identification of the theropod, which made the bite traces, e.g., the ichnotaxon *Linichnus serratus* Jacobsen and Bromley, 2009 and *Knethichnus parallelum* Jacobsen and Bromley, 2009. This is because theropod denticles are species-specific, thereby allowing the serration patterns to be matched with the denticle morphology of teeth from the theropod fossil record. *Linichnus serratus* is characterised by a serrated edge, while the trace *Knethichnus parallelum* consists of parallel lines across an area of the substrate (e.g., bone). By feeding Komodo dragons with goat carcasses, D'Amore and Blumenschine (2012), found that the teeth of Komodo dragons were indeed capable of producing the *Knethichnus parallelum* ichnotaxon, a finding that strengthens the usefulness of an ichnotaxon as a tool for understanding feeding behaviour from trace fossils. On rare occasions, stronger evidence of predator-prey interaction can be found, such as a tooth directly embedded in a fossil bone (Currie and Jacobsen, 1995; DePalma *et al.*, 2013).

Visual inspection assisted by microscopy has revealed important details in ichnotaxa. However, intrinsically limited to surface observations, visual inspection does not reveal internal structures. Fourteen years ago, Ketcham and Carlson (2001) provided an excellent description of computed tomography (CT) and potential applications of CT in the geosciences. Here, the present authors therefore provide only a summary of the most relevant physics and the techniques underlying CT.

As an X-ray-based imaging technique, CT provides cross-sectional images of the scanned object in a process that does not disturb the internal structures. The source of x-rays, i.e. the Röntgen tube, the x-ray detector and supplementary electronics, rotate around the scanner bed, located in the centre of the system. Some of the electromagnetic radiation is absorbed or scattered by the scanned object and does not reach the detector. Multi-angle x-ray projections of the scanned object are acquired, while the object is simultaneously moved slowly through the x-ray beam by a motor-

ised scanner bed, resulting in a dataset of information on spatially distributed back-projected x-ray attenuation. The attenuation information is reconstructed to two-dimensional cross-sectional images, representing the x-ray attenuation in grey scales. By convention, the x-ray absorption unit (i.e. the CT-number) is measured in Hounsfield units (HU), which give the present x-ray attenuation relative to the x-ray attenuation of water. Typical medical CT systems work in a limited 12-bit HU-range of –1024 to +3071. Because the attenuation of water is low, relative to materials containing heavy elements, e.g., bone (calcium), rock (silicon), and metals, the conventional Hounsfield scale is potentially inappropriate for the CT imaging of fossils. However, using a scaling procedure, the conventional Hounsfield scale can be rescaled by a factor of 10 at the cost of relative image contrast because the HU depth is still restrained to 12 bits, resulting in HU steps of 10 HU in the extended Hounsfield scale (Kolz *et al.*, 1990; Link *et al.*, 2000; Coolens and Childs, 2003). This expands the density range of CT and can be beneficial, when scanning large solid specimens and potentially fossils.

One aspect of studies on the feeding behaviour of carnivorous dinosaurs is whether active hunting or scavenging prevailed (DePalma *et al.*, 2013). Although the answer to this interesting question is speculative in nature, evidence of a healed bite trace with or without embedded teeth would indicate that active hunting occurred.

Bone healing in mammals is well described and takes place in several phases (Geneser, 2002). The first three phases involve the formation of non-calcified tissue and are therefore not likely to be preserved in fossilised specimens. The formation of woven bone commences in about one week after the bone damage, whereas the formation of lamellar bone takes place after 6 weeks. Subsequently, the bone can undergo further remodelling. Although the bone growth and repair processes are likely to be different in dinosaurs and mammals, there is evidence of repair processes from all major dinosaur groups, including different stages of callus formation, resembling the patterns seen in mammalian, reptilian and avian species (Straight *et al.*, 2009). Callus formation denotes a process, in which soft, fibrous tissue advances into the traumatised zone, where it mineralises during weeks after the trauma. This callus zone is often recognisable according to its morphology, appearing externally as mineralised sheet/crests around the fracture zone with grainy patches nonparallel to the long axis of the bone and internally displaying characteristic differences in the developed trabeculated network. These processes are temporally divided in such a way that mineralisation appears only weeks, months or even years after traumatisation. Identification of the repair stage, including identification of the callus stage, and healed woven, and lamellar bone, provide clues on the magnitude of the healing and therefore the survival period after traumatisation. In this study, a distal fragment of a dinosaur femur bone displaying several distinct bite traces was thoroughly examined, using a clinical-like approach, including pathoforensic visual inspection of surface traces, supplemented by CT evaluation. The authors apply the hypothesis that one lesion on the femur fragment could possibly be healed and may, therefore, be a re-

sult of an early non-fatal attack, while all other lesions are bite traces, resulting from a final, fatal attack and/or *post mortem* scavenging.

MATERIALS AND METHODS

The bone fragment (length: 18 cm, width: 9.5–14.5 cm, depth: 7.7 cm, volume: 1,295.5 cm^3, weight: 3,009.6 g; Fig. 1 and Supplementary Material 1) is a Hadrosauridae sp. distal femur fragment, which was an uncatalogued specimen from the collection at The Royal Tyrrell Museum of Palaeontology, Alberta, Canada. The fragment was donated by certificate to the main author (ARJ) in 1993, in connection with research collaboration to aid further research. Because this study focuses on methodology, the geological setting and species information are not relevant.

Visual inspection and stereomicroscopy

The first appearance of a fossilised dinosaur specimen is naturally in the field, where interesting trace fossils may be difficult to identify using only a brief visual examination. Bite traces can be very hard to distinguish from trample marks and other bone erosion traces. Accordingly, there is a great risk that relevant specimens will be overlooked and never studied. Bones in collections also have the potential to bear important feeding traces that have simply been missed owing to the limitations of visual inspection, as it takes a trained eye to identify the relevant details. In this study, a stereomicroscope (Olympus, SZ-CTV) was used to enhance interpretation of minute anatomical structures, relevant to the identification of possible bone healing.

CT imaging

The bone fragment was CT scanned using a dual-source clinical CT system (Siemens Somatom Definition; Siemens Medical Solutions, Forchheim, Germany). To investigate and optimize acquisition parameters, 16 co-registered scans were performed, applying different tube voltages (80, 100, 120 and 140 kV) and slightly different current×time product (850 and 900 mAs). Image resolution was 322×322× 600 μm^3 and the scan duration was approximately 83 s, depending on the settings used. Acquired projections were reconstructed using different convolution kernels: B40s (Heart View smooth), B46s (Heart View sharp), B50s, B60s. The Siemens kernel abbreviations reflect kernel type, e.g., "B" for body, image sharpness represented by numbers (where a high number, e.g. "60", is sharp and a low number, e.g. "40", is smooth), and scan mode, where e.g. "s" represent the standard mode.

Silicon-rich fossils are high-density structures, compared to non-fossilised bone structures, typically examined with x-ray CT in a clinical setting; therefore, the authors tested data acquisition with an extended CT scale in several scans. Acquired images were compared subjectively by means of visual inspection by a radiologist (BF) to determine which acquisition parameters were the most useful for fossil bone visualisation. Additionally, a profile analysis
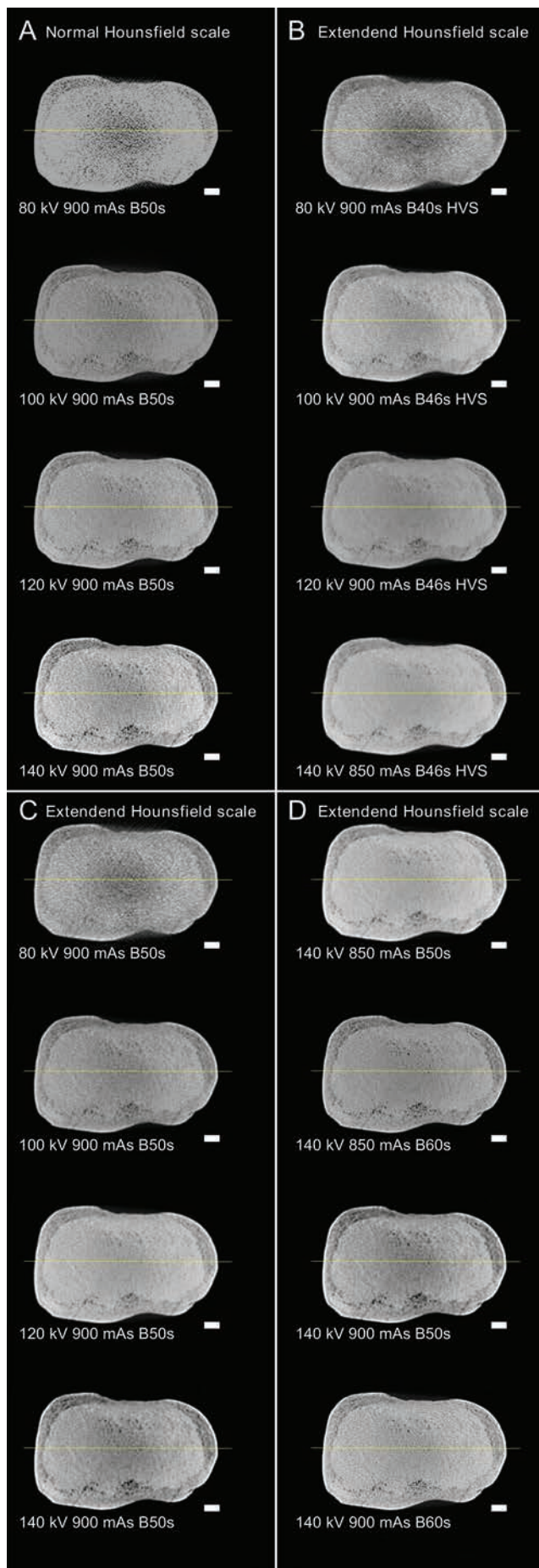
was carried out by recording the density distribution for profiles, placed in the same position in all acquired scans (for profile placement see Fig.1).

CT-generated sections through the bite traces on the fossilised bone were examined for evidence of callus formation or bone reconstruction. The surfaces of the two major bite traces were segmented using the Amira 5.6 software package (Amira 3D Software for Life Sciences, http://www. fei.com/software/amira-3d-for-life-sciences/) to generate a surface reconstruction of the bite trace, i.e., a negative of the tip of the tooth that delivered the trace. Bite-trace reconstructions were merged with a three-dimensional virtual reconstruction of the specimen, generated from 61 consecutive high-resolution photos from different angles. These were compiled in the freeware software Autodesk 1 2 3 Catch (Autodesk 123D Catch, Generate 3d model from photos, http://www.123dapp.com/catch), ultimately generating an interactive three-dimensional model of the specimen and bite trace, saved as an interactive .PDF file (Supplementary Material 1). Additionally, the bite-trace reconstructions were 3-D-printed using a Makerbot Replicator 2 Desktop 3D Printer (Stratasys, New York, USA) as scale models (100% and 400% scaling) in polylactic acid plastic.

RESULTS

A comparison of the fossilised bone visualised and examined with traditional visual inspection, stereomicroscopy and x-ray CT, respectively, is shown in Fig. 1. In addition to the description of the specimen, the authors provide a supplementary file, containing an interactive three-dimensional model of the fossil specimen, which can be visualised in 3D and interactively manipulated in normal freeware .PDF readers (see Supplementary Material 1).

Visual inspection of the bone revealed post-sedimentation cracks caused by rock pressure and several lesions. The focus was on six lesions, namely two large (lesions 1 and 2 in Fig. 1A) and three minor (lesions 4, 5 and 6 in Fig. 1A) with no filling. Additionally, the appearance of one filled, apparently circular lesion (lesion 3 in Fig. 1A) was especially interesting, owing to possible signs of healing. The bone fibres seemed to be crushed around the lesions (1, 2, 4, 5, and 6 in Fig. 1A) and they were classified as bite traces. These bite traces did not show evidence of healing through the formation of new bone. Bite traces 1 and 2 were assigned to the ichnotaxon *Nihilichnus nihilicus* (Mikuláš *et al.*, 2006) because of their morphology. Visual examination

Fig. 2. Optimisation of x-ray computed tomography parameters *via* visual inspection. The similar section (see Fig. 1D for section placement) of 16 different scans with varying acquisition parameters. Low tube voltage (80 kV) results in scale max out, using the normal 12-bit CT scale (**A**) and in x-ray attenuation (hypo-dense middle part of the section). Applying the extended CT scale resolves the problem of scale max out (**B**, **C**, **D**). A sharp kernel (B60s) *vs*. a smooth kernel (B40s) yield slightly sharper images and a high current×time product increases signal to noise ratio. Scale bar is 1 cm.
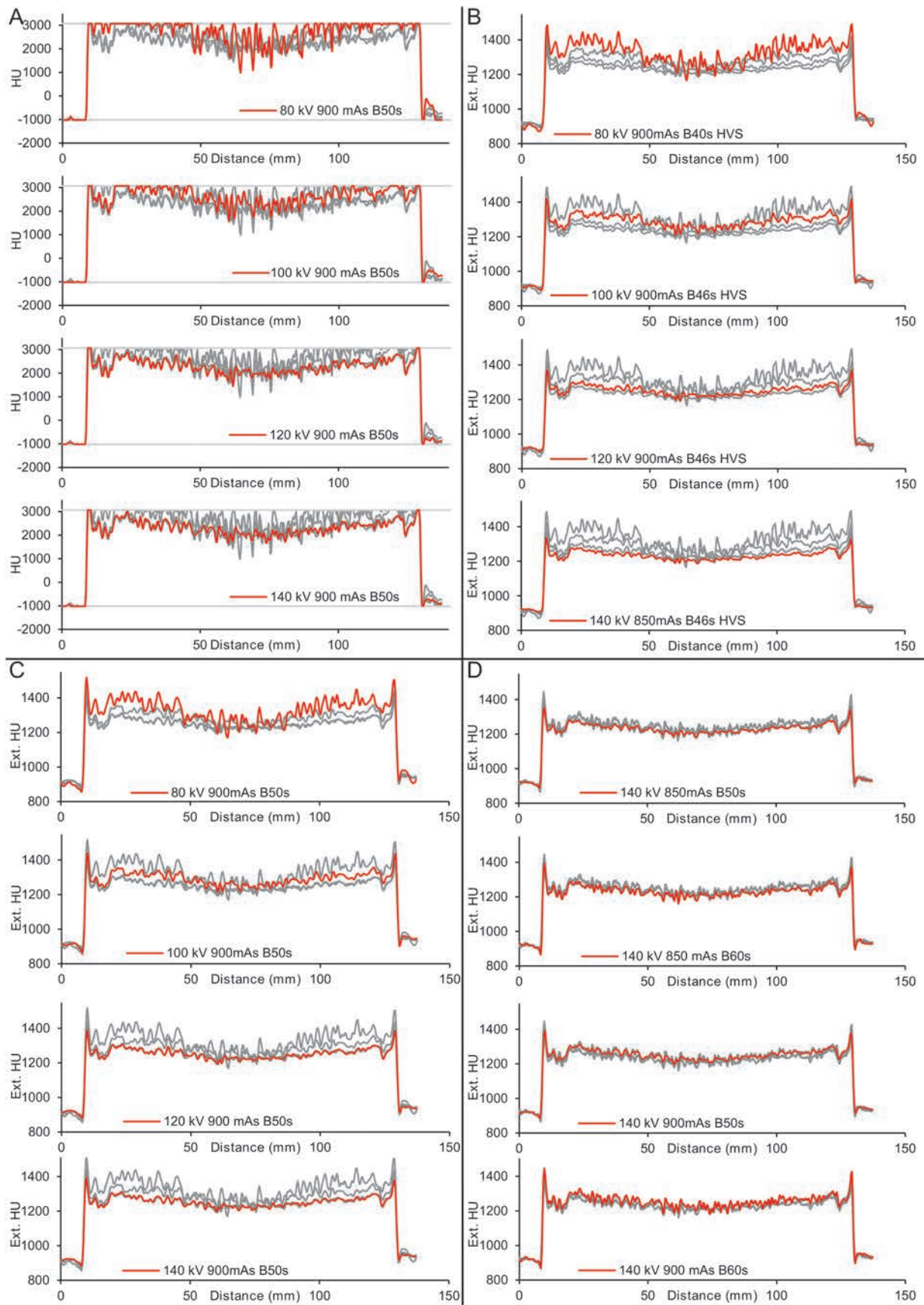
Fig. 3.   Optimisation of x-ray computed tomography parameters *via* density distribution profile plots. Profile plots through the 16 sections in Fig. 2 (profile placement indicated by yellow line in Fig. 2). Low tube voltage (80 kV) results in scale max out, using the normal 12-bit CT scale (**A**) and in x-ray attenuation (valley in mid-portion of profiles). Applying the extended CT scale resolves the problem of scale max out (**B**, **C**, **D**).

alone and stereomicroscopy were not sufficient to incontestably conclude whether lesion 3 is actually healed and/or if a tooth could be imbedded in the structure. Therefore, CT was used to examine the internal morphology of the fossil.

CT acquisition was optimised using 16 co-registered scans with varying acquisition parameters (Fig. 2). Visual inspection of all scans by a radiologist showed that choosing a high tube voltage, 140 kV, and a high current×time product, 900 mAs, in combination with a sharp convolution kernel (B60s) and the extended CT scale, resulted in sectional images with optimal image contrast between the different anatomical compartments and a high signal-to-noise ratio (see bottom image in Fig. 2D).

For an objective evaluation of the effect of different acquisition parameters, the authors recorded density distribution profiles from the similar section in all 16 different scans (Fig. 3). Applying the conventional Hounsfield scale resulted in the HU cut-off of high intensities above 3071 HU at low tube voltages (Fig. 3A), whereas applying the extended CT scale resolved this problem (Fig. 3B–D). Applying smooth *versus* sharp convolution kernels only resulted in minor differences between the density distribution profiles (compare Fig. 3B, C). Applying a low tube voltage resulted in significant x-ray attenuation, affecting deep structures in the sample, which appeared as a hypointense (i.e. dark) zone in the middle of the sample (Fig. 2) and accordingly as a valley in the mid-portion of the density profile plots (Fig. 3); this artefact, however, was counteracted completely by increasing the tube voltage. Additionally, increasing the current×time product from 850 mAs to 900 mAs resulted in an increased signal-to-noise ratio. The reader is invited to compare the two curves in Fig. 3D, obtained at 140 kV 850 mAs B60s and 140 kV 900 mAs B60s, respectively. The 900 mAs curve rides on top of the 850 mAs curve, as a result of a slightly higher signal.

CT was used to generate sections through the bite traces of the fossil specimen and obtain high-resolution images of the internal morphology (Fig. 4). A radiologist performed visual inspection of the CT-generated images that clearly displayed a radio-dense peripheral cortical layer (Figs 2, 4) and internal cancellous (i.e., trabecular or spongy) bone structures (Fig. 4). CT imaging revealed the same three major bone lesions at the surface of the bone as visual inspection by a forensic examiner (Fig. 4A). Lesion 1 measured 12 mm in width, while lesion 2 measured 10 mm and appeared clearer and more sharply defined than lesion 1 (Fig. 4A). The bone fractures of lesions 1 and 2 appeared to have the same direction and were 6 and 10 mm deep, respectively. The cortical layers of lesions 1 and 2 have evidently been broken and their subcortical bone densities were hyperdense, indicating that the corticalis and the subcortical bone have been compressed. Lesions 4, 5 and 6 (Fig. 4A, B) were minor and all displayed an intact cortical layer. Lesion 3 (Fig. 4A) was 3 mm deep centrally and displayed a sharply defined lesion in the cortical layer, 20 mm wide. However, the subcortical bone and the underlying cancellous bone did not confirm signs of compression and appeared unchanged by comparison with neighbouring areas of the fossil, thereby contradicting the visual impression that lesion 3 could display signs of bone formation and healing. Further-

more, CT revealed evidence that no tooth remnants or other foreign objects were located in association with lesion 3 or any of the five other bite traces (Fig. 4).

DISCUSSION

The present study describes a clinical-like methodology including a pathomorphological investigation and CT examination of the internal structures of a fossil dinosaur bone specimen, bearing bite traces. The approach applied was suitable for testing and rejecting the original hypothesis of the authors, namely that the present bone specimen displayed two different types of trace; i.e. several distinct *post mortem* bite traces and one possibly healed bite trace, maybe even with an imbedded tooth.

The owner of the specimen (ARJ) wanted to clarify whether the circular lesion (3 in Figs 1A, 4A) was a potentially healed structure. However, microscopic enlargement of the lesion and a sound pathomorphological interpretation reject this otherwise very interesting hypothesis. Differences in growth patterns between dinosaur and mammalian bones have indeed been identified. For example, bone ossification in mammals happens from an epiphyseal plate, whereas endochondral ossification in the juxtaarticular cartilage is present in extant saurians and possibly functioned similarly in dinosaurs (Golder and Christian, 2002). Even with possible differences in growth rate taken into account, the evidence of healing in lesion 3 is too sparse to conclude that there was more than one week of survival after a possible predator-prey interaction. If the animal was alive one week or more after the trauma, lesion 3 could be expected to display evidence of bony callus, either in the subperiosteal region or deeper in the lesion (Straight *et al.*, 2009). However, none of these findings was evident, when the fossil was carefully examined by means of the stereomicroscope.

While microscopy and high-resolution pictures in combination with dental putty casts can be utilised to cost-effectively create representative models of fossil bite traces, they are intrinsically restricted to surface inspection. Hence, previous studies have used CT to visualise the internal morphology of dinosaur bones (e.g., Straight *et al.*, 2009; Boyd *et al.*, 2013; DePalma *et al.*, 2013) and to estimate pterosaur skeletal mass (Martin and Palmer, 2014). In the present study, CT imaging was also employed to rule out the possibility of an imbedded tooth in lesion 3 (Fig. 4; e.g., Currie and Jacobsen, 1995; DePalma *et al.*, 2013). Additionally, CT imaging conclusively revealed that lesion 3 does not display callus formation, indicating that no bone repair occurred following injury. Lesions 4, 5 and 6 displayed intact cortical layers and the subcortical layers in these lesions were less hyperdense, compared to the deeper bite traces (compare lesions 4, 5 and 6 to lesions 1 and 2 in Fig. 4A, B), indicating that CT can be used to identify at least relative differences in bite force and the morphology of bite traces.

By appreciating the fundamental physics underlying CT modality, appropriate settings can be chosen to prevent image artefacts and misinterpretation of the resulting morphology (Ketcham and Carlson, 2001). Accordingly, the authors speculate whether the hypodense core of the fossil left
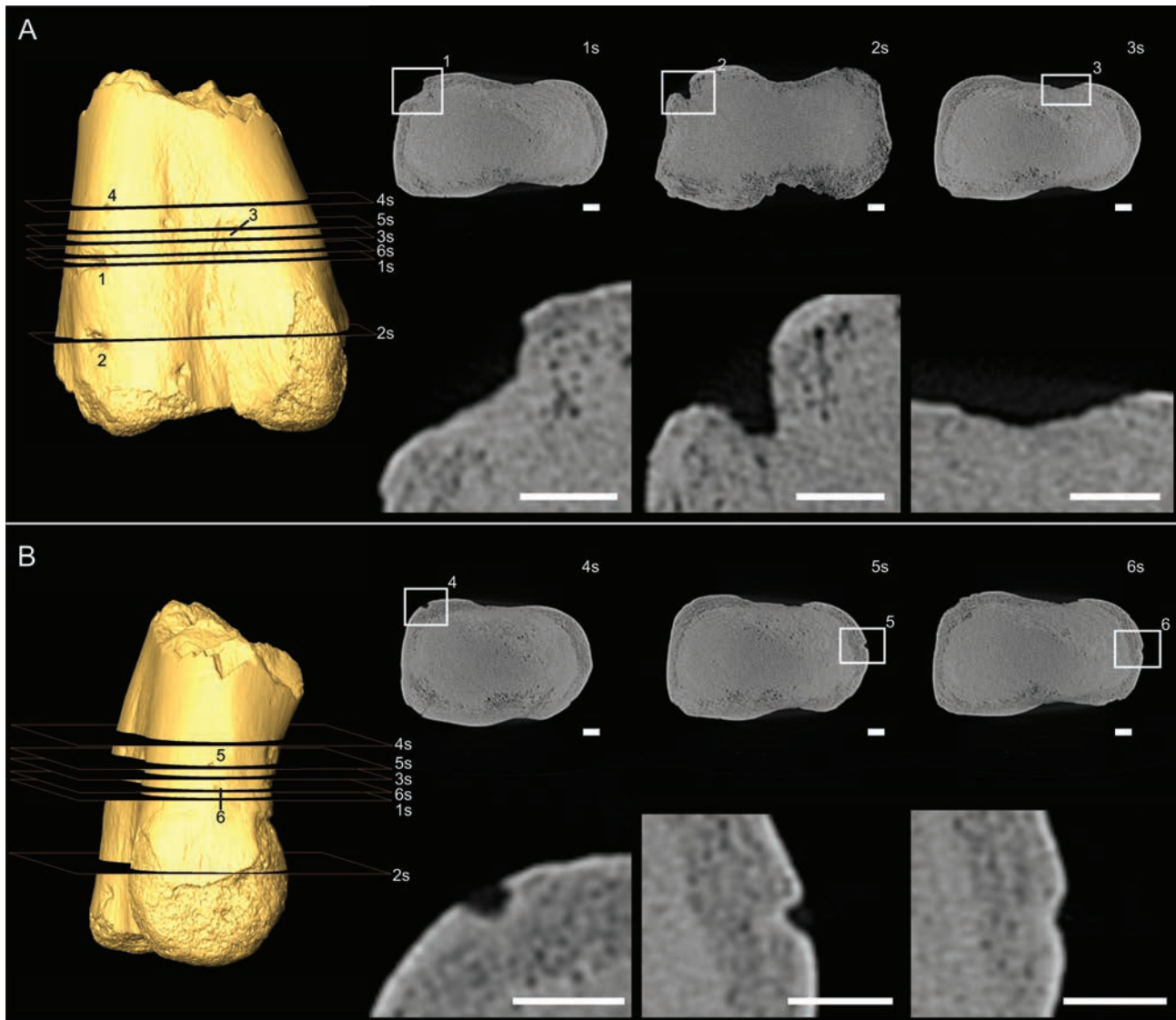
Fig. 4.   Inspection of bite trace using x-ray computed tomography. Sections through six lesions (i.e. bite traces) on the fossilised specimen. The peripheral cortical layer and internal cancellous structure are clearly visible. Lesions are numbered from 1–6 and associated sections from 1s-6s. **A.** Lesions 1 and 2 display broken cortical layers and hyperdense signals in the subcortical region, possibly indicating that the bite event caused significant compression of the underlying bone tissue. **B.** Lesions 4, 5 and 6 differ from 1 and 2 in their intact cortical layer, but do appear slightly hyperdense subcortically, compared to neighbouring structures. The cortical layer is absent from lesion 3, which does not display noticeable signal change below the surface. Scale bar is 1 cm.

femur of *Dysalotosaurus lettow-vorbecki* (e.g., fig. 2C in Golder and Christian, 2002) is the result of x-ray attenuation due to an energy limitation of the 120 kV x-rays used to penetrate the specimen, rather than a precise visualisation of the internal morphology of the specimen. If used with respect to the inherent limitations in x-ray absorbance by fossil-material, CT data can aid effective communication of key data through genuine digital representation of internal and external anatomy, including the production of interactive 3-D models. For example, the reader could open Supplementary material 1 in a standard .PDF reader and explore the interactive features (see information in p. 464). As well, it is even possible to recreate structures that are physically missing (i.e. "negative"), exemplified here by the two 3-D prints (Fig. 1A and B) that unequivocally revealed the tooth-like morphologies of lesion 1 and 2.

CONCLUSIONS

CT imaging is an excellent adjunctive tool to traditional visual inspection and microscope methodology, used in the examination of fossil dinosaur bones. This study showed that the utilisation of a clinical-like examination procedure, including pathoforensic examination and CT evaluation, could reject the hypothesis that the bone fragment under study displayed signs of post-traumatic healing. Although proper stereomicroscopic examination identified missing key features of bone regeneration, invisible to the non-expert, the CT scans proved especially useful for determination of the morphologies of six different lesions. A comparison of different CT settings clearly showed that high tube voltages and current×time product are advantageous, owing to extensive x-ray attenuation in the mineralised fossil.

Also, the extended CT scale can expand the density-quantitative range.

The authors encourage researchers in geology, palaeontology, anthropology, and zoology to apply interactive files to aid the communication of complex objects under study. In this study, the authors used traditional photography and freeware software to generate the interactive Supplementary Material 1. Additionally, 3-D print files of key structures could potentially be published as material that is supplementary to scientific articles, because they are easily distributed in contrast to, for example, dental putty models. This is useful, as most people optimally interpret intricate morphological structures (e.g., tooth and jaw morphology, joint structures, resonance chambers, etc.) through "seeing with the hands". This effort has become realistic because 3-D printing is now widely affordable through the introduction of simple, low-cost desktop printers (Barnatt, 2013).

Acknowledgments

REFERENCES

Amira 3D Software for Life Sciences, http://www.fei.com/software/amira-3d-for-life-sciences/

Autodesk 123D Catch, Generate 3D Model from Photos, http://www.123dapp.com/catch

Barnatt, C., 2013. *3D Printing: The Next Industrial Revolution*. Printed and bound by ExplainingTheFuture.com.

Boyd, C. A., Drumheller, S. K. & Gates, T. A., 2013. Crocodyliform feeding traces on juvenile ornithischian dinosaurs from the Upper Cretaceous (Campanian) Kaiparowits Formation, Utah. *PlosOne,* 8(2):e57605. doi: 10.1371/journal.pone.0057605.

Coolens, C. & Childs, P. J., 2003. Calibration of CT Hounsfield units for radiotherapy treatment planning of patients with metallic hip prostheses: the use of the extended CT-scale. *Physics in Medicine and Biology,* 48: 1591–1603.

Currie, P. J. & Jacobsen, A. R., 1995. An azhdarchid pterosaur eaten by a velociraptorine theropod. *Canadian Journal of Earth Sciences*, 32: 922–925.

D'Amore, D. C. & Blumenschine, R. J., 2012. Using striated tooth marks on bone to predict bodysize in theropod dinosaurs: a model based on feeding observations of *Varanus komodoensis,* The Komodo monitor. *Paleobiology,* 38: 79–100.

DePalma, R. A., II, Burnham, D. A., Martin, L. D., Rothschild, B. M. & Larson, P. L., 2013. Physical evidence of predatory behavior In Tyrannosaurus rex. *Proceedings of the National Academy of Sciences of the United States of America,* 110: 12560–12564.

Erickson, G. M. & Olson, K. H., 1996. Bite marks attributable to *Tyrannosaurus rex*: Preliminary description and implications. *Journal of Vertebrate Paleontology*, 16: 175–178.

Erickson, G. M., Van Kirk, S. D., Su, J., Levenston, M. E., Caler, W. E. & Carter, D. R., 1996. Bite-force estimation for *Tyrannosaurus rex* from tooth-marked bones. *Nature*, 382: 706–708.

Fiorillo, A. R., 1991. Prey bone utilization by predatory dinosaurs. *Palaeogeography, Palaeoclimatology, Palaeoecology*, 88: 157–166.

Geneser, F., 2002. *Histologi – på molekylærbiologisk grundlag.* Munksgaard, Viborg [In Danish.]

Golder, W. & Christian, A., 2002. Quantitative CT of dinosaur bones. *Journal of Computer Assisted Tomography*, 26: 821–824.

Jacobsen, A. R., 1998. Feeding behaviour of carnivorous dinosaurs as determined by tooth marks on dinosaur bones. *Historical Biology*, 13: 17–26.

Jacobsen, A. R. & Bromley, R. G., 2009. New ichnotaxa based on tooth impression on dinosaur and whale bones. *Geological Quarterly*, 53: 373–382.

Ketcham, R. A. & Carlson W. D., 2001. Acquisition, optimization and interpretation of X-raycomputed tomographic imagery: applications to the geosciences. *Computer & Geosciences*, 27: 381–400.

Klotz, E., Kalender, W. A., Sokiransky, R. & Felsenberg, D., 1990. Algorithms for the reduction of CT artifacts caused by metallic implants. *Proceedings of SPIE, Medical Imaging*, 1234: 642–640.

Link, T. M., Berning, W., Scherf, S., Joosten, U., Joist, A., Engelke, K. & Daldrup-Link, H. E., 2000. CT of metal implants: Reduction of artifacts using an extended CT scale technique. *Journal of Computer Assisted Tomography*, 24: 165–172.

Martin, E. G. & Palmer, C., 2014. A novel method of estimating pterosaur skeletal mass using computed tomography scans. *Journal of Vertebrate Paleontology*, 34: 1466–1469.

Mikuláš, R., Kadlecová, E., Fejfar, O. & Dovořák, Z., 2006. Three new ichnogenera of biting and gnawing traces on reptilian and mammalian bones: A Case study from the Miocene of the Czech Republic. *Ichnos*, 13: 113–127.

Njau, J. K. & Blumenschine, R. J., 2012. Crocodylian and mammalian carnivore feeding traces on hominid fossils from FLK 22 and FLK NN 3, Plio-Pleistocene, Olduvai Gorge, Tanzania. *Journal of Human Evolution*, 63: 408–417.

Pirrone, C. A., Buatois, L. A. & Bromley, R. G., 2014. Ichnotaxoobases for bioerosion trace fossils in bones. *Journal of Paleontology*, 88: 195–203.

Rogers, R. R., Krause, D. W. & Rogers, K. C., 2003. Cannibalism in the Madagascan dinosaur *Majungatholus atopus. Nature*, 422: 515–518.

Straight, W. H., Davis, G. L., Skinne, H. C. W., Haims, A., McClennan, B. L. & Tanke, D. H., 2009. Bone lesions in Hadrosaurs: computed tomographic imaging as a guide for paleohistologic and stable-isotopic analysis. *Journal of Vertebrate Paleontology*, 29: 315–325.

Supplementary material 1. Interactive 3-D model of fossil specimen. The interactive .PDF file should be viewed in Adobe Acrobat Reader 9 or higher. To activate the 3-D feature, left-click the model. Using the cursor, it is now possible to rotate, zoom, pan the model and in the model tree, all segments of the model can be turned on/off or made transparent. The model displays all external structures used for visual inspection, and additionally segmentations of two "negative" tooth marks. The scale cube is 1×1×1 cm. (http://www.asgp.pl)